Hindawi Publishing Corporation
Advances in Materials Science and Engineering
Volume 2015, Article ID 291230, 7 pages
http://dx.doi.org/10.1155/2015/291230

*Research Article*

# Effect of $Eu^{3+}$ Concentration on the Luminescent Properties of $SrTiO_3$ Phosphors Prepared by Pressure-Assisted Combustion Synthesis

**C. R. García,[1] J. Oliva,[2] M. T. Romero,[1] R. Ochoa-Valiente,[1] and L. A. Garcia Trujillo[1]**

[1]*Universidad Autónoma de Coahuila, Facultad de Ciencias Físico Matemáticas, Unidad Camporredondo, 25280 Saltillo, COAH, Mexico*
[2]*Centro de Investigaciones en Óptica, Apartado Postal 1-948, 37150 León, GTO, Mexico*

Correspondence should be addressed to C. R. García; deschamps2001@hotmail.com

Received 3 May 2015; Revised 3 August 2015; Accepted 5 August 2015

Academic Editor: Amit Bandyopadhyay



This work presents the structural, morphological, and luminescent characterization of pure $SrTiO_3$ and $SrTiO_3$:$Eu^{3+}$ powders doped with different europium atomic concentrations from 3.0 to 7.0 a.t.%. Those phosphors were prepared by pressure-assisted combustion synthesis using titanium oxide as precursor and were subjected to postannealing at 1200°C. XRD measurements indicated that undoped and $Eu^{3+}$ doped samples presented a single cubic crystalline phase and SEM images demonstrated that we have particles with sizes in the range of 0.2 $\mu$m–1.0 $\mu$m. Moreover, the size of the grains increases as the content of $Eu^{3+}$ dopant increases. A strong red emission from $Eu^{3+}$ ions was obtained by photoluminescence under excitation at 396 nm and confirmed by cathodoluminescence. All those results indicate that our red phosphors could be useful for potential applications in solid state lighting and field emission displays.

## 1. Introduction

During last years, oxide materials doped with rare earths (REs) have attracted great attention because they can be excited with infrared and ultraviolet light (300–420 nm) to produce red, green, and blue emissions [1–3]. In addition, those doped materials could be useful to enhance the color rendering index (CRI) in fluorescent lamps and phosphor converted LEDs (Pc-LEDs) [4]. White light emission with high brightness in solid state devices (SSL) can be created by a blend of three phosphors (red, green, and blue) or a single material emitting a broad band of visible light [5, 6]. Luminescent oxides are phosphors which possess higher physical and chemical stability in comparison to traditional luminescent materials based on sulfur and phosphorus and are also interesting because they could be synthesized with low cost methods and most of them are not toxic [7]. Furthermore, white lighting sources such as fluorescent lamps which use these oxide phosphors have great color stability and do not suffer strong changes in chromaticity and color rendering because intrarare earth atomic transitions are very stable even with changes of temperature, specifically at the working temperatures of the SSL [8]. A common oxide phosphor commercially used for applications in lighting and field emission displays is $Y_2O_3$; when it is doped with $Eu^{3+}$ and $Tb^{3+}$, green and red emissions are possible under UV excitation [9, 10]. This phosphor is very efficient for the generation of light with a quantum efficiency of nearly 100% [11], but scientists are focusing energies currently to find new materials which combine magnetic, ferroelectric, low toxicity, and luminescent properties (multifunctional materials) and those additional properties cannot be provided by $Y_2O_3$ host. Some previous works have found that $SrTiO_3$:$Pr^{3+}$ and $SrTiO_3$:$Eu^{3+}$ phosphors are potential candidates as red phosphors with good paramagnetic properties [12–16]. In particular, studies have shown that $SrTiO_3$:$Eu^{3+}$ is a good absorber in the long ultraviolet region and it is an oxide material with high chemical stability [14]. Besides, strontium titanate doped with

rare earths (REs) is a compound widely studied due to its high dielectric constant (~300) and ferroelectric properties, which make $SrTiO_3$:RE a multifunctional material [14]. Several techniques to produce $SrTiO_3:Eu^{3+}$ powders include the solid state reaction method, synthesis from molten chloride complex salts, and the sol-gel technique [14–16]. However, the pressure-assisted combustion synthesis (PACS) technique has not been used to obtain $Eu^{3+}$ doped $SrTiO_3$ to the best of our knowledge and this technique has been used successfully to produce highly luminescent materials by changing their size and morphology [17–19]. Also, the as-synthesized powders obtained by PACS have higher surface area, which in turn improves the photoluminescence due to surface phenomena. Hence, this work presents the use of the PACS method with a pressure of 2.7 MPa to synthesize pure $SrTiO_3$ and $SrTiO_3:Eu^{3+}$powders with different atomic concentrations (a.t.%) of Eu. Moreover, this work demonstrates that the use of the PACS method allowed us to introduce a high content of europium without quenching the luminescence. Finally, the morphology, crystalline structure, and cathodoluminescence properties were studied as a function of $Eu^{3+}$ content.

## 2. Experimental

*2.1. Synthesis of $SrTiO_3$ and $SrTiO_3:Eu^{3+}$ Powders.* Pure $SrTiO_3$ and $SrTiO_3$:Eu powders were synthesized by pressure-assisted combustion synthesis (PACS) using strontium nitrate [$Sr(NO_3)_3{\cdot}H_2O$ Puratronic 99.9965%], europium nitrate [$Eu(NO_3)_3{\cdot}6H_2O$ REacton 99.9%], and titanium oxide [$TiO_2$ anatase phase Alfa Aesar, 99.5%] as reagents and hydrazine [$N_2H_4$ Alfa Aesar de 98.5%] as the reductive noncarbonaceous fuel. The pure $SrTiO_3$ powders were synthesized using two different precursors as a source of titanium in order to know which one is better to obtain pure phase under our conditions of synthesis: titanium dioxide ($TiO_2$) and titanium isopropoxide [$Ti(OC_3H_7)_4$]. The chemical reactions are expressed in

$$\begin{aligned} &2(1-x)\,Sr(NO_3)_2 + 2xEu(NO_3)_3 + 2TiO_2 \\ &\quad + (5+3x)\,N_2H_4 \longrightarrow 2Sr_{1-x}Eu_xTiO_3 \\ &\quad + 2(5+3x)\,H_2O + (7+4x)\,N_2 \end{aligned} \tag{1}$$

$$\begin{aligned} &(1-x)\,Sr(NO_3)_2 + xEu(NO_3)_3 + Ti(OC_3H_7)_4 \\ &\quad + (11-3x)\,N_2H_4 \longrightarrow Sr_{1-x}Eu_xTiO_3 \\ &\quad + (36-6x)\,H_2O + (12-0.5x)\,N_2 + CO_2 \end{aligned} \tag{2}$$

The samples obtained from these precursors are labeled as STO and $STO_{iso}$, respectively. The europium doped samples were synthesized using $TiO_2$, and $Eu^{3+}$ was added in atomic concentration of $x$ = 3.0%, 5.0%, and 7.0%; those samples were labeled as STO3, STO5, and STO7, respectively. The precursors were weighed at the appropriate stoichiometric ratio ($\Phi$ = 1) and dissolved in deionized water [20]. The mixture obtained was homogeneous and had a gelatinous consistency. Later, the mixture was introduced into a high pressure reactor. The reactor was purged with argon for 10 minutes to create an inert atmosphere, and subsequently it was closed. After this, the temperature was raised at 100°C and the argon flow began again for about 15 minutes in order to evacuate the water vapor. Afterwards, the reactor exhaust was closed and the argon inlet opened to pressurize up to 2.7 MPa. The next step was to increase gradually the reactor temperature up to 340°C and it was maintained for 15 minutes to produce an exothermic reaction in a pressurized environment. When the temperature reached 340°C, a maximum peak on the pressure of 7.0 MPa was observed during the combustion reaction. Once the reaction has occurred, the exhaust valve was carefully opened to release the pressure and the reactor was purged with argon in order to remove any residual gas. To understand the advantages of the pressure-assisted process, an Eu-doped sample with $x$ = 7.0 a.t.% was fabricated by normal combustion synthesis without applying pressure using hydrazine; this sample was named STO7-CS. The concentration of 7% for $Eu^{3+}$ dopant was selected for the sample synthesized without pressure because the sample STO7 fabricated with pressure presented the best luminescent properties. Finally, all powders were removed from the pressure reactor and annealed at 1200°C in air atmosphere.

*2.2. Morphological and Structural Characterization.* The X-ray diffraction patterns of the samples were obtained using a Philips X'Pert diffractometer with $CuK_\alpha$ radiation ($\lambda$ = 0.15406 nm) in the $2\theta$ range of 10–80° (steps of 0.02°) at room temperature. Scanning electron microscopy (SEM) images were obtained utilizing energy of 10 kV in a JEOL JSM-530 microscope.

*2.3. Optical Characterization.* Photoluminescence (PL) spectra were collected with a fluorescence spectrophotometer (Hitachi FL-4500). Cathodoluminescence (CL) was measured with a spectrometer consisting of a 0.25 m monochromator (Oriel MS260i) and a thermoelectrically cooled CCD (InstaspecIV). The spectrometer was coupled with a quartz optic fiber to an ultrahigh vacuum (UHV) CL chamber equipped with a 10 keV electron gun (Kimball Physics). The luminance and the CIE coordinates of our phosphors under an excitation of 8 $\mu$W were obtained using a Konica Minolta spectroradiometer CS-2000. All the measurements were made at room temperature.

## 3. Results and Discussion

*3.1. Structure and Morphology.* The $SrTiO_3$ (STO) compound has a perovskite-type structure with space group *Pm3m* (221) and lattice parameter of $a$ = 3.905 Å. Furthermore, it is an insulator at room temperature with a direct band gap value of 3.2 eV [21]. The diffraction pattern of STO powders in Figure 1(b) indicates the presence of a single cubic phase which is in agreement with the JCPDS 86-0178 card, while the $STO_{iso}$ sample (see Figure 1(a)) showed small peaks of secondary phases identified as $TiO_2$ and $Sr_3Ti_2O_7$, which are indexed with $\alpha$ and $\beta$ symbols, respectively. This

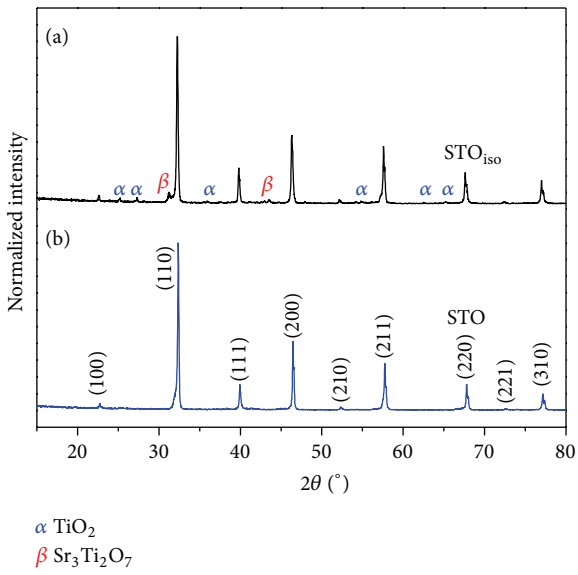


Figure 1: XRD patterns of (a) STO$_{iso}$ and (b) STO sample.

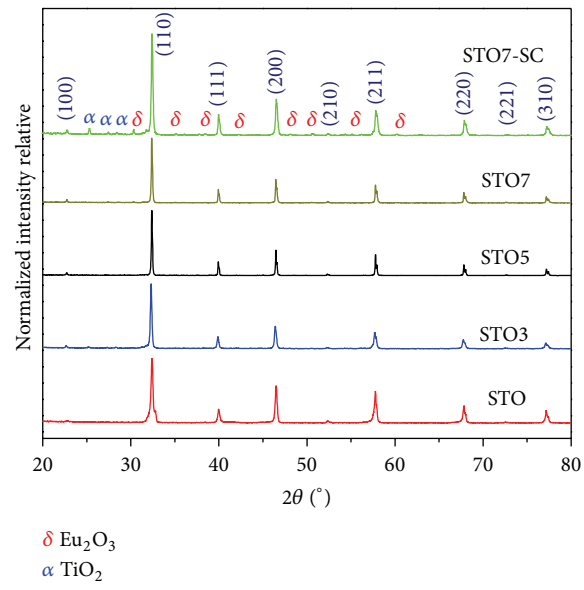


(a)

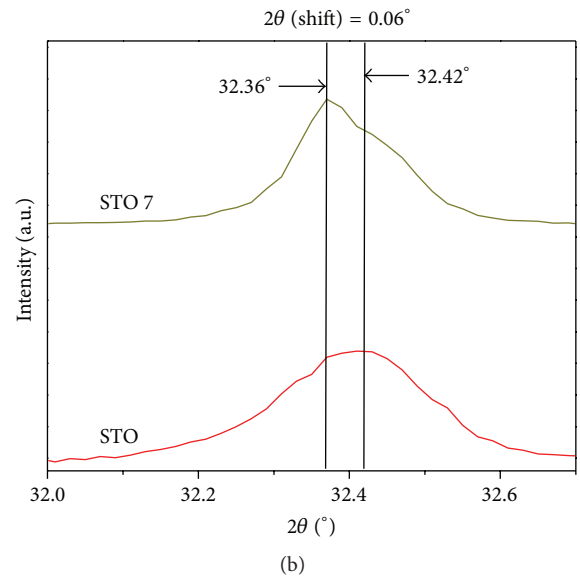


(b)

Figure 2: (a) XRD patterns of (a) STO, STO3, STO5, and STO7 phosphors. (b) shows the diffraction peaks associated with the plane (110) for samples STO and STO7.

means that the use of titanium isopropoxide as precursor produces additional spurious phases; in contrast, the titanium oxide produced pure $SrTiO_3$. Thus, the europium doped materials were fabricated using the titanium oxide to avoid impurities. Probably, the spurious phases appeared because the temperature of 340°C is barely enough to burn the organic compounds from the titanium isopropoxide; then, the presence of organic residuals could change the dynamics of the reaction to form pure $SrTiO_3$. In contrast, the inorganic precursor $TiO_2$ does not have organic materials which can interfere with the chemical reaction to produce pure $SrTiO_3$. The XRD patterns of pure $SrTiO_3$ (STO) and $Eu^{3+}$ doped $SrTiO_3$ (STO:$Eu^{3+}$) powders in Figure 2 show that all samples had only cubic phase. The presence of a single phase in all samples suggests that $Eu^{3+}$ ions are successfully substituting the $Sr^{2+}$ or $Ti^{4+}$ into the $SrTiO_3$ crystalline lattice [13, 14]. Moreover, this result also indicates that our procedure of synthesis is good enough to introduce relatively high concentrations of Eu dopant into STO without producing segregation of phase. Furthermore, the XRD patterns of the sample STO7-SC produced without pressure ($P = 0$) were compared with that one for sample STO7 in order to elucidate the advantages of the pressure-assisted process. Figure 2(a) shows that sample STO7-SC presented spurious phases, marked by $\delta$ and $\alpha$ symbols, attributed to $Eu_2O_3$ and $TiO_2$, respectively. This result points out that $Eu^{3+}$ cannot be successfully incorporated into the crystal lattice of $SrTiO_3$ without applying pressure. Thus, the pressure-assisted combustion synthesis allows us to obtain the $SrTiO_3$ phosphors with cubic phase without any impurity; see sample STO7 in Figure 2(a). The lattice parameters were calculated taking in account the $2\theta$ position of the diffraction peak associated with the plane (110) on the XRD patterns and Bragg's law. Therefore, the estimated lattice parameters were $a = 3.9035$ Å, 3.9090 Å, 3.9071 Å, and 3.9051 Å for STO, STO3, STO5, and STO7, respectively, and those values are very close to the reported value of 3.905 Å [22].

The substitution of $Sr^{2+}$ ions by $Eu^{3+}$ can induce a charge decompensation as has been reported [14]; this result can distort the crystalline lattice which could enhance the luminescence intensity of $SrTiO_3$:$Eu^{3+}$ because the interatomic 4f-4f $Eu^{3+}$ forbidden transitions are more probable in lattices with no inversion of symmetry [17]. Thus, the crystalline lattice is distorted by the charge decompensation and by the difference between the atoms sizes of the $Eu^{3+}$ (1.087 Å) and $Sr^{2+}$ (1.44 Å); this has been observed in several perovskite systems [14–16, 22–24]. A measure of the distortion of a perovskite-type $ABO_3$ lattice can be determined by using the

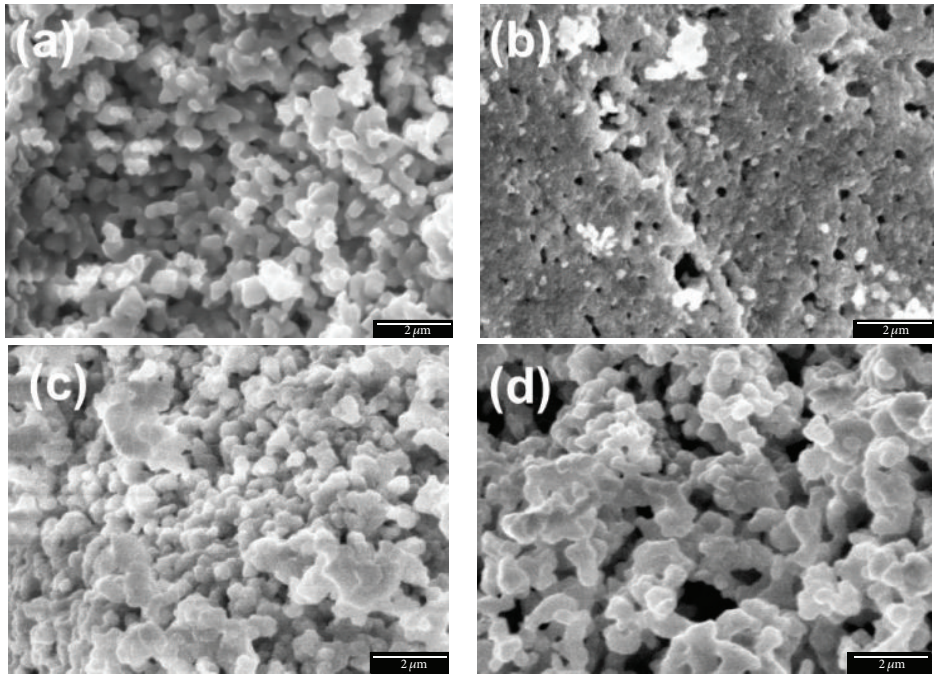


Figure 3: SEM images of (a) STO, (b) $STO_{iso}$, (c) STO3, and (d) STO7 samples.

Goldsmith tolerance factor ($t$) that depends on the ionic radii $r_A$, $r_B$, and $r_O$ of the perovskite $ABO_3$ structure [24] and is given by the following equation:

$$t = \frac{r_A + r_0}{\sqrt{2}\,(r_B + r_0)}. \tag{3}$$

If we substitute the values $r_A$ ($Sr^{2+}$) = 1.44 Å, $r_B$ ($Ti^{4+}$) = 0.605 Å, and $r_0$ ($O^{-2}$) = 1.40 Å corresponding to the pure $SrTiO_3$ cubic perovskite [25], we obtain a tolerance factor of $t = 1.0$ which corresponds to an ideal perovskite; this value indicates that the positions of the atoms into the pure $SrTiO_3$ have high symmetry. The incorporation of $Eu^{3+}$ to substitute $Sr^{2+}$ ions should change the tolerance factor $t$; if we calculate the tolerance factor using $r_B$ ($Eu^{3+}$) = 1.087 Å, a value $t = 0.87$ is obtained; this points out that the introduction of $Eu^{3+}$ as dopant into the crystalline lattice causes a huge distortion. The pure $SrTiO_3$ structure is formed by $TiO_6$ octahedral anions within the cubic lattice. The $Sr^{2+}$ or $Eu^{3+}$ ions are surrounded by eight $TiO_6$ octahedrons in the $SrTiO_3$:$Eu^{3+}$ matrix; thus, the $TiO_6$ anions should be distorted in the perovskite structure $SrTiO_3$:$Eu^{3+}$ by the doping effect of $Eu^{3+}$; in consequence, the sites where the $Eu^{3+}$ ions are located within the crystal lattice of STO lack symmetry. This is beneficial for our powders because the photoluminescence properties are enhanced [14–16]. The imbalance of the crystalline structure can also be observed by a shift of the diffraction peaks in the XRD patterns. Figure 2(b) depicts the diffraction peaks corresponding to plane (110) in samples STO and STO7. As observed, there is a shift toward lower angles of the diffraction peak associated with plane (110) as the Eu concentration is increased from 0 to 7%. The difference in $2\theta$ was 0.06°. Hence, we can infer that the crystal lattice has been expanded due to the presence of Eu and it was similarly observed in [14].

SEM images of STO, $STO_{iso}$, STO3, and STO7 samples are illustrated in Figures 3(a)–3(d), respectively. All of them (except sample $STO_{iso}$ in Figure 3(b)) exhibited individual and coalesced grains with irregular shape. The average sizes for those grains were 0.48 $\mu$m, 0.56 $\mu$m, and 0.60 $\mu$m for STO, STO3, and STO7, respectively. Our results are in agreement with other reports where authors showed that the coalescence of grains is favored with a successive increase of the $Eu^{3+}$ content [26]. The sample $STO_{iso}$ in Figure 3(b) exhibits almost all particles coalesced in comparison with the rest of samples, and the few grains that are not coalesced have an average size of ~0.23 $\mu$m; the absence of individual grains could be due to the low level of crystallinity and presence of other phases as explained in section above. Finally, it is worthy to mention that the sample STO7-SC shows coalesced grains as observed for $STO_{iso}$ in Figure 3(b) but the size of the grains that are not coalesced was 0.44 $\mu$m; this result corroborates that the coalescence of grains is related with the poor crystallinity of the sample STO7-SC and, therefore, spurious phases such as $Eu_2O_3$ and $TiO_2$ were observed in the sample STO7-SC; see Figure 2(b).

*3.2. Luminescent Properties.* Figure 4 shows the excitation spectra of the STO3, STO5, and STO7 samples monitored at 593 nm. A main excitation band is centered at 396 nm and corresponds to the $^5F_0 \rightarrow {}^7L_6$ transition of $Eu^{3+}$. It is worthy to notice that there is no charge transfer band (CTB) in the range of 200–300 nm which associated with the transfer of electrons between $O^{2-}$ and $Eu^{3+}$ atoms. The no presence is normally caused by a quenching effect produced by a high content of $Eu^{3+}$ ions, since those ones absorb the excitation

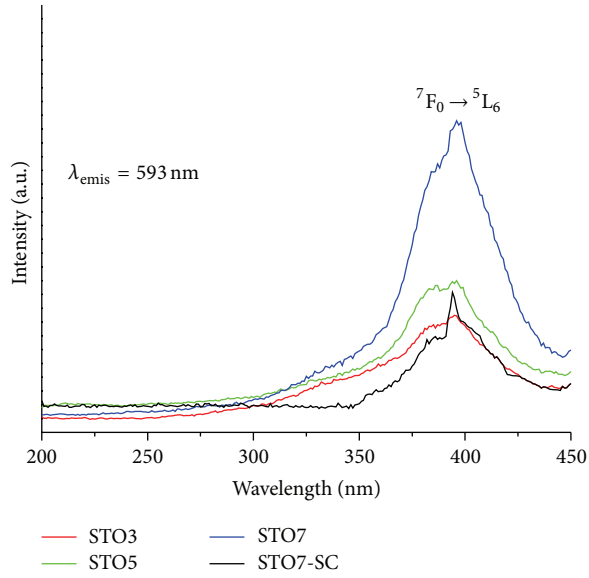


Figure 4: Excitation spectra of samples STO3, STO5, STO7, and STO7-SC.

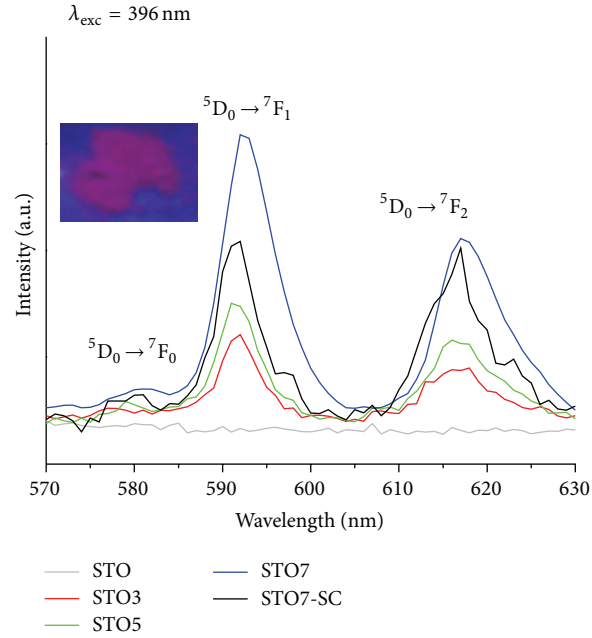


Figure 5: Emission spectra of samples STO, STO3, STO5, STO7, and STO7-SC.

of light preferably [14]. Also the excitation band is broader and asymmetric as the $Eu^{3+}$ dopant concentration increases. This is probably due to the increase of lattice distortions as the amount of Eu increases and to the band gap transitions of the host as similarly observed in BiOCl:Eu [27]. The emission spectra of the STO3, STO5, and STO7 samples in Figure 5 show two main peaks located at 593 nm and 615 nm as well as a small shoulder at 581 nm. The first peak is associated with the magnetic dipole transition $^5D_0 \rightarrow {}^7F_1$, the second one corresponds to an electric dipole transition $^5D_0 \rightarrow {}^7F_2$, and the shoulder is related with the singlet-singlet forbidden transition $^5D_0 \rightarrow {}^7F_0$ [13–17]. This figure also depicts the no emission of the undoped sample STO as well as an increase of luminescence as the content of $Eu^{3+}$ increases, suggesting that we have not reached the quenching of luminescence even though we used a dopant concentration as high as 7.0 a.t.%, which is opposite to that observed in the work of Jiang et al., where they observed quenching after a concentration of 5.0 a.t.% [14]. Further, Figure 5 shows that the sample fabricated without pressure (sample STO7-CS) presented an intensity 43% lower with respect to the sample made with pressure (sample STO7). This result confirms that the PACS method is useful to enhance the luminescent properties of the samples. The excitation spectrum of sample STO7-CS in Figure 4 indicates that the position and shape of the excitation band did not change, suggesting that the crystalline distortions of this sample should be similar to those of sample STO7. The inset in Figure 5 illustrates the red emission of sample STO7 which had the strongest luminescence; this sample was excited utilizing a commercial 396 nm UV-LED with a power of 8 $\mu$W and its luminance observed was ~250 $Cd/m^2$; this level of brightness of our phosphors is enough for applications in displays and lighting [28]. The CIE coordinate was (0.57, 0.42), indicating that the emission color is located in the orange-red region.

It is well known that the narrow bands in the luminescent spectrum of $Eu^{3+}$ are sensitive to the crystallographic site symmetry occupied by $Eu^{3+}$ ions; that is, the electric dipole transition $^5D_0 \rightarrow {}^7F_2$ observed at 615 nm is allowed only when $Eu^{3+}$ is located at a noncentrosymmetric crystallographic site, while the $^5D_0 \rightarrow {}^7F_1$ magnetic dipole transition observed at 593 nm comes from Eu ions in sites with inversion symmetry. Usually the luminescence intensity ratio of $^5D_0 \rightarrow {}^7F_2$ to $^5D_0 \rightarrow {}^7F_1$, also called asymmetry ratio, is considered as a probe to detect the inversion symmetry around $Eu^{3+}$ ions in the host [29]. In our case, the values for this ratio were 0.75, 0.77, and 0.68 for the STO3, STO5, and STO7 samples, suggesting that the degree of distortion decreases as the Eu concentration increases; we would expect higher distortions in the lattice as the $Eu^{3+}$ increases but it did not occur. This opposite behavior can be explained if the europium enters into $Sr^{2+}$ and $Ti^{4+}$ sites at the same time as observed by Jiang et al. [14]. In addition, a low degree of distortions can be supported by the fact that the values of the cell parameters for STO and STO7 were similar (3.9035 for STO and 3.9051 Å for STO7), which indicates that the lattice distortions in STO7 are small. In fact, the difference in the values of cell parameters in the samples STO3 and STO5 with respect to that for STO was higher (3.9090 Å, and 3.9071 Å for STO3 and STO5, resp.), suggesting that the crystalline distortions are bigger in those samples; this is in agreement with the values of luminescence intensity ratio for STO3 and STO5. The $^5D_0 \rightarrow {}^7F_1$ transition (emission centered at 593 nm) is very sensitive to the chemical bonds in the vicinity of $Eu^{3+}$; if the distortions in sample STO are small, a higher intensity of this band is expected compared to that for $^5D_0 \rightarrow {}^7F_2$ transition which hardly changes due to any variation in the crystalline lattice around the $Eu^{3+}$

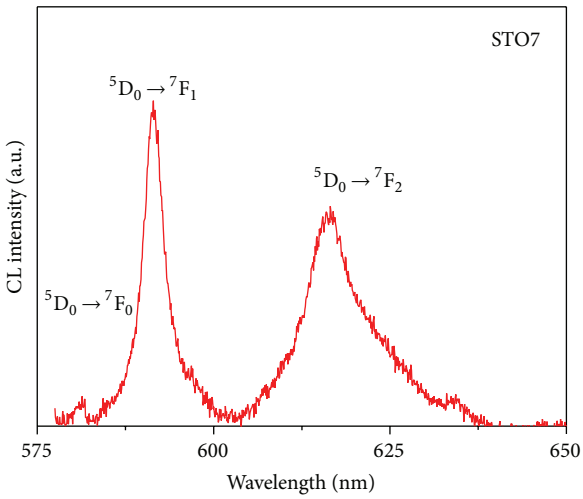


FIGURE 6: Cathodoluminescence spectra of sample STO7.

ion. Jiang et al. also presented a similar spectrum to that we have in our work [14], where higher emission intensity was observed for the $^5D_0 \rightarrow {}^7F_1$ transition compared to that for the $^5D_0 \rightarrow {}^7F_2$ transition. Finally, we should mention that the emission corresponding to the $^5D_0 \rightarrow {}^7F_0$ transition observed in our spectra in Figure 5 is rarely presented in Eu-doped hosts. This emission is only observed in hosts where the site symmetries of $Eu^{3+}$ are low [30]. In fact, it is well known that the substitution of divalent ions by trivalent ions produces a distortion of the site symmetry which allows a strong interaction of the $^5D_0$ and $^7F_0$ levels [30]. In our case, the $Eu^{3+}$ is surely entering into the $Sr^{2+}$ sites; this in turn promotes the $^5D_0 \rightarrow {}^7F_0$ transition.

The cathodoluminescence spectrum of STO7 sample is presented in Figure 6. As observed, the spectrum is very similar to that obtained by photoluminescence and the emission color was orange-red again. This confirms that the origin of the luminescence of this material is associated with the $Eu^{3+}$ dopant, since the transitions $^5D_0 \rightarrow {}^7F_0$, $^5D_0 \rightarrow {}^7F_1$, and $^5D_0 \rightarrow {}^7F_2$ appear again. In this case, the ratio $^5D_0 \rightarrow {}^7F_2 / {}^5D_0 \rightarrow {}^7F_1$ was 0.70; from here, we can infer that the $^5D_0 \rightarrow {}^7F_2$ transition is improved in cathodoluminescence. If we compare that transition in photoluminescence (emission band at 617 nm) with that in cathodoluminescence, we realize that such a band is broader in cathodoluminescence and this explains why the ratio $^5D_0 \rightarrow {}^7F_2/{}^5D_0 \rightarrow {}^7F_1$ increased in comparison with photoluminescence. By the way, cathodoluminescence is a method which requires electrons with high energy to excite any material; thus, they can penetrate the bulk material easily to excite more $Eu^{3+}$ ions. Therefore, we observed a higher contribution to the red emission of $Eu^{3+}$ ions in cathodoluminescence. Finally, those results confirm that the $Eu^{3+}$ ions were incorporated successfully inside the lattice using our pressure-assisted combustion method, since the same red emission bands were observed in cathodoluminescence and in photoluminescence; this last one involves the excitation of $Eu^{3+}$ ions located at the surface on microparticles.

## 4. Conclusions

In summary, $SrTiO_3$ and $SrTiO_3$:$Eu^{3+}$ powders were successfully produced by pressure-assisted combustion synthesis; this method allowed us to introduce $Eu^{3+}$ up to 7 a.t.% without quenching of luminescence. All samples presented a cubic structure and there was no segregation of phases when the samples are fabricated with $TiO_2$ as precursor or up to a concentration of 7 a.t.% for the europium dopant. However, segregation of phases appeared when titanium isopropoxide is used as reagent or when the pressure-assisted process is not used. Further, the luminescence properties of the phosphors are improved by increasing the concentration of europium or by using the pressure-assisted process. The luminance of 250 $Cd/m^2$ observed in the sample with 7 a.t.% of $Eu^{3+}$ suggests that our phosphors could be useful for applications in solid state lighting where UV sources are employed or displays.

## Conflict of Interests

The authors declare that there is no conflict of interests regarding the publication of this paper.

## Acknowledgments

The authors appreciate the excellent technical work performed by E. Aparicio, F. Ruiz, I. Gradilla, J. A. Diaz, E. Flores, C. Albor, C. Gonzalez, M. Sainz, J. A. Peralta, P. Casillas, G. Vilchis, and J. Palomares. C. R. García acknowledges F-PRODEP-SEP-38/Rev-03/SEP-23-005 Funds and CGEPI-UAdeC for supporting this research. C. R. García thanks C. Méndez for their helpful discussions.

## References

[1] Q. Liu, Y. Liu, Z. Yang, X. Li, and Y. Han, "UV-excited red-emitting phosphor $Eu^{3+}$-activated $Ca_9Y(PO_4)_7$," *Spectrochimica Acta A: Molecular and Biomolecular Spectroscopy*, vol. 87, pp. 190–193, 2012.

[2] Z. Xia, J. Zhou, and Z. Mao, "Near UV-pumped green-emitting $Na_3(Y,Sc)Si_3O_9$:$Eu^{2+}$ phosphor for white-emitting diodes," *Journal of Materials Chemistry C*, vol. 1, no. 37, pp. 5917–5924, 2013.

[3] X. Zhao, L. Fan, T. Yu, Z. Li, and Z. Zou, "High efficient blue emission of $Ce^{3+}$ activated $Ca_4P_2O_9$ phosphor for white LEDs," *Optics Express*, vol. 21, no. 25, pp. 31660–31667, 2013.

[4] C. Shen, Y. Yang, S. Jin, and H. Feng, "Synthesis and luminous characteristics of $Ba_2MgSi_{2-x}Al_xO_7$: $0.1Eu^{2+}$, $0.1Mn^{2+}$ phosphor for WLED," *Optik*, vol. 121, no. 1, pp. 29–32, 2010.

[5] J. K. Sheu, S. J. Chang, C. H. Kuo et al., "White-light emission from near UV InGaN–GaN LED chip precoated with blue/green/red phosphors," *IEEE Photonics Technology Letters*, vol. 15, no. 1, pp. 18–20, 2003.

[6] A. Žukauskas, R. Vaicekauskas, and M. S. Shur, "Colour-rendition properties of solid-state lamps," *Journal of Physics D: Applied Physics*, vol. 43, no. 35, Article ID 354006, 2010.

[7] V. Sivakumar and U. V. Varadaraju, "Intense red-emitting phosphors for white light emitting diodes," *Journal of the Electrochemical Society*, vol. 152, no. 10, pp. H168–H171, 2005.

[8] E. F. Schubert and J. K. Kim, "Solid-state light sources getting smart," *Science*, vol. 308, no. 5726, pp. 1274–1278, 2005.

[9] K. Mishra, N. K. Giri, and S. B. Rai, "Preparation and characterization of upconversion luminescent $Tm^{3+}/Yb^{3+}$ co-doped $Y_2O_3$ nanophosphor," *Applied Physics B*, vol. 103, no. 4, pp. 863–875, 2011.

[10] T. Anh, P. Benalloul, C. Barthou, L. T. Giang, N. Vu, and L. Minh, "Luminescence, energy transfer, and upconversion mechanisms of y 2 O 3 nanomaterials doped with $Eu^{3+}$, $Tb^{3+}$, $Tm^{3+}$, $Er^{3+}$, and $Yb^{3+}$ ions," *Journal of Nanomaterials*, vol. 2007, Article ID 48247, 10 pages, 2007.

[11] A. Paulraj, P. Natarajan, K. Munnisamy et al., "Photoluminescence efficiencies of nanocrystalline versus bulk $Y_2O_3$:Eu phosphor—revisited," *Journal of the American Ceramic Society*, vol. 94, no. 5, pp. 1627–1633, 2011.

[12] H. Yamamoto, S. Okamoto, and H. Kobayashi, "Luminescence of rare-earth ions in perovskite-type oxides: from basic research to applications," *Journal of Luminescence*, vol. 100, no. 1–4, pp. 325–332, 2002.

[13] I. K. Battisha, A. Speghini, S. Polizzi, F. Agnoli, and M. Bettinelli, "Molten chloride synthesis, structural characterisation and luminescence spectroscopy of ultrafine $Eu^{3+}$-doped $BaTiO_3$ and $SrTiO_3$," *Materials Letters*, vol. 57, no. 1, pp. 183–187, 2002.

[14] C. Jiang, L. Fang, M. Shen, F. Zheng, and X. Wu, "Effects of Eu substituting positions and concentrations on luminescent, dielectric, and magnetic properties of $SrTiO_3$ ceramics," *Applied Physics Letters*, vol. 94, Article ID 071110, 2009.

[15] I. W. Lenggoro, C. Panatarani, and K. Okuyama, "One-step synthesis and photoluminescence of doped strontium titanate particles with controlled morphology," *Materials Science and Engineering: B*, vol. 113, no. 1, pp. 60–66, 2004.

[16] S. P. Feofilov, A. A. Kaplyanskii, A. B. Kulinkin, and R. I. Zakharchenya, "Nanocrystalline SrTiO3:$Eu^{3+}$ and $BaTiO_3$:$Eu^{3+}$: fluorescence spectroscopy and optical studies of structural phase transitions," *Physica Status Solidi (C)*, vol. 4, no. 3, pp. 705–710, 2007.

[17] O. Ozuna, G. A. Hirata, and J. McKittrick, "Luminescence enhancement in $Eu^{3+}$-doped $\alpha$- and $\alpha$-$Al_2O_3$ produced by pressure-assisted low-temperature combustion synthesis," *Applied Physics Letters*, vol. 84, no. 8, pp. 1296–1298, 2004.

[18] M. J. Oviedo, O. Contreras, C. E. Rodriguez, Z. S. MacEdo, G. A. Hirata, and J. McKittrick, "Photo- and radioluminescence characteristics of bismuth germanate nanoparticles by sol-gel and pressure-assisted combustion synthesis," *Optical Materials*, vol. 34, no. 7, pp. 1116–1119, 2012.

[19] O. Ozdemir, S. Zeytin, and C. Bindal, "A study on NiAl produced by pressure-assisted combustion synthesis," *Vacuum*, vol. 84, no. 4, pp. 430–437, 2009.

[20] J. McKittrick, L. E. Shea, C. F. Bacalski, and E. J. Bosze, "The influence of processing parameters on luminescent oxides produced by combustion synthesis," *Displays*, vol. 19, no. 4, pp. 169–172, 1999.

[21] D. Kan, R. Kanda, Y. Kanemitsu et al., "Blue luminescence from electron-doped $SrTiO_3$," *Applied Physics Letters*, vol. 88, no. 19, Article ID 191916, 2006.

[22] J. H. Haeni, P. Irvin, W. Chang et al., "Room-temperature ferroelectricity in strained $SrTiO_3$," *Nature*, vol. 430, no. 7001, pp. 758–761, 2004.

[23] H. J. Kim, U. Kim, T. H. Kim et al., "Physical properties of transparent perovskite oxides (Ba,La)$SnO_3$ with high electrical mobility at room temperature," *Physical Review B*, vol. 86, no. 16, Article ID 165205, 2012.

[24] C. Li, K. C. K. Soh, and P. Wu, "Formability of $ABO_3$ perovskites," *Journal of Alloys and Compounds*, vol. 372, no. 1-2, pp. 40–48, 2004.

[25] C. Jaisuk and M. Suewattana, "Structural and electronic properties of Mn doped $SrTiO_3$ by first principles calculations," *Thai Journal of Physics*, vol. 10, Article ID 170011, pp. 170011–170014, 2014.

[26] O. Contreras, S. Srinivasan, F. A. Ponce, G. A. Hirata, F. Ramos, and J. McKittrick, "Microstructural properties of Eu-doped GaN luminescent powders," *Applied Physics Letters*, vol. 81, no. 11, pp. 1993–1995, 2002.

[27] Y. Li, Z. Zhao, Z. Song et al., "Far-red-emitting BiOCl:$Eu^{3+}$ phosphor with excellent broadband NUV-excitation for white-light-emitting diodes," *Journal of the American Ceramic Society*, vol. 98, pp. 1–7, 2015.

[28] J. A. Wheatley, G. J. Benoit, J. E. Anderson et al., "Efficient LED light distribution cavities using low loss, angle-selective interference transflectors," *Optics Express*, vol. 17, no. 13, pp. 10612–10622, 2009.

[29] F. Gu, C. Zhong Li, and H. Bo Jiang, "Combustion synthesis and photoluminescence of MgO:$Eu^{3+}$ nanocrystals with $Li^+$ addition," *Journal of Crystal Growth*, vol. 289, no. 1, pp. 400–404, 2006.

[30] H. J. Seo, B. K. Moon, B. J. Kim, J. B. Kim, and T. Tsuboi, "Optical properties of europium ions in $SrB_2O_4$ crystal," *Journal of Physics Condensed Matter*, vol. 11, no. 39, pp. 7635–7643, 1999.